Available online at www.sciencedirect.com
ScienceDirect
Journal of Sound and Vibration 324 (2009) 916–939
JOURNAL OF SOUND AND VIBRATION
www.elsevier.com/locate/jsvi

Vibration absorption in systems with a nonlinear energy sink: Nonlinear damping

Y. Starosvetsky, O.V. Gendelman*

Faculty of Mechanical Engineering, Technion – Israel Institute of Technology, Haifa 32000, Israel

Received 14 August 2008; received in revised form 11 February 2009; accepted 16 February 2009
Handling Editor: M.P. Cartmell
Available online 5 April 2009

Abstract

In this work, response regimes are investigated in a system comprising of a linear oscillator (subject to harmonic excitation) and a nonlinear energy sink (NES) with nonlinear damping characteristics. An analytical technique for the treatment of certain class of nonlinear damping functions is developed. Special attention is paid to the case of piecewise-quadratic damping, motivated by possible applications. It is demonstrated that the NES with a properly tuned piecewise-quadratic damping element allows complete elimination of undesirable periodic regimes. In this way, an efficient system of vibration absorption is obtained, and its performance can overcome that of a tuned mass damper (TMD). Numerical results agree satisfactorily with the analytical predictions.

1. Introduction

Nonlinear strategies in vibration suppression have been extensively studied over the last three decades. One popular solution in vibration mitigation is the introduction of a weakly nonlinear vibration absorber. This solution is based on the addition of a weakly nonlinear dof to a main system given to various types of external excitation [1–11]. The effective bandwidth is governed by the damping in the absorber and a tradeoff exists between attenuation efficiency and bandwidth.

Systems comprised of linear substructures and essentially nonlinear attachments are also intensively studied from the viewpoint of vibration mitigation. Irreversible transient transfer (pumping) of energy from the substructure to the essentially nonlinear attachment (nonlinear energy sink (NES)) was demonstrated and studied in Refs. [12–15]. In the same papers, it has been shown that, when properly designed, essentially nonlinear local attachments may passively absorb energy from transiently loaded linear subsystems, acting as *NESs*.

Addition of a relatively small and spatially localized nonlinear attachment (NES) leads to essential changes in the properties of the entire system. Unlike common linear and weakly nonlinear systems, systems with strongly nonlinear elements are able to react efficiently to the amplitude characteristics of external forcing over a rather wide range of frequencies [15–18]. The spectacular abilities of the NES to suppress limit cycle

*Corresponding author.
E-mail address: ovgend@tx.technion.ac.il (O.V. Gendelman).

0022-460X/$ - see front matter © 2009 Elsevier Ltd. All rights reserved.
doi:10.1016/j.jsv.2009.02.052

oscillations in the van der Pol oscillator has been demonstrated in Ref. [19]. Other experimental and analytical studies [20,21] have shown that the NES may be of use in suppression of aero-elastic instabilities.

Recent studies concerned with application of NES to linear/weakly nonlinear systems subject to harmonic excitations [22–25] have revealed an unusual response regime referred to as a strongly modulated regime (SMR). As was demonstrated in Refs. [22,25], the SMR is rather effective for vibration suppression. Numerical, experimental, and analytical studies related to this type of response are reported in Refs. [22–28].

Despite the obvious advantages of NES applications over their linear and weakly nonlinear counterparts, some drawbacks also exist. The main drawback common to systems containing nonlinearities is the existence of additional branches of periodic regimes that may be disastrous for vibration absorption. These regimes may lead to vibrations with amplitudes much higher than those of the linear subsystems without the attachment are.

In this paper, we develop the strategy of elimination of the undesired periodic regimes in a system comprised of a linear oscillator subject to harmonic excitation and the NES. This strategy is based on application of nonlinear damping with piecewise-quadratic characteristics instead of the commonly used linear (viscous) element. General analytical treatment of the system with a generic nonlinear damping function is presented in the second section. NES with piecewise-quadratic damping characteristics is considered in Section 3, together with a detailed analytical study of response regimes in the system. The tuning procedure of damping parameters for elimination of the unwanted periodic regimes is discussed in Section 4. Numeric verification of the developed methodology is performed in Section 5. Section 6 is devoted to concluding remarks and discussion.

2. Description of the model and analytic treatment

Following previous studies [22–28], we consider the linear oscillator subject to harmonic excitation and attached to a NES comprised of an essentially nonlinear (pure cubic) spring and symmetric nonlinear damping elements. The system is described by the following equations:

$$\ddot{y}_1 + \varepsilon f(y_1 - y_2, \dot{y}_1 - \dot{y}_2) + y_1 + \tfrac{4}{3}\varepsilon(y_1 - y_2)^3 = \varepsilon A\cos((1+\varepsilon\sigma)t)$$

$$\varepsilon\ddot{y}_2 - \varepsilon f(y_1 - y_2, \dot{y}_1 - \dot{y}_2) - \tfrac{4}{3}\varepsilon(y_1 - y_2)^3 = 0 \tag{1}$$

By replacement of variables:

$$y_1 + \varepsilon y_2 = u$$

$$y_1 - y_2 = w \tag{2}$$

the system described by Eq. (1) is transformed to the following form:

$$\ddot{u} + \frac{u + \varepsilon w}{1+\varepsilon} = \varepsilon A\cos((1+\varepsilon\sigma)t)$$

$$\ddot{w} + (1+\varepsilon)f(w, \dot{w}) + \frac{u + \varepsilon w}{1+\varepsilon} + \frac{4}{3}(1+\varepsilon)w^3 = \varepsilon A\cos((1+\varepsilon\sigma)t) \tag{3}$$

Complex variables are introduced as

$$\dot{u} + \mathrm{i}u = \varphi_1 \mathrm{e}^{\mathrm{i}t}$$

$$\dot{w} + \mathrm{i}w = \varphi_2 \mathrm{e}^{\mathrm{i}t} \tag{4}$$

The system under investigation is considered in the vicinity of 1:1 resonance, and it is therefore reasonable to assume that both φ_1 and φ_2 vary slowly with respect to unit frequency. It means that they describe slow modulation of functions u and w, respectively. Thus, substituting Eq. (4) into Eq. (1), and performing averaging over one forcing period, one obtains

$$\dot{\varphi}_1 + \frac{\mathrm{i}\varepsilon}{2(1+\varepsilon)}(\varphi_1 - \varphi_2) = \frac{\varepsilon A}{2}\exp(\mathrm{i}\varepsilon\sigma t)$$

$$\dot{\varphi}_2+\frac{\mathrm{i}\varepsilon}{2(1+\varepsilon)}(\varphi_2-\varphi_1)+(1+\varepsilon)a_1(\varphi_2,\varphi_2^*)-\frac{\mathrm{i}(1+\varepsilon)}{2}|\varphi_2|^2\varphi_2=\frac{\varepsilon A}{2}\exp(\mathrm{i}\varepsilon\sigma t)$$

$$a_1(\varphi_2,\varphi_2^*)=\frac{1}{2\pi}\int_0^{2\pi}f(w,\dot{w})\mathrm{e}^{-\mathrm{i}t}\,\mathrm{d}t \tag{5}$$

where $a_1(\varphi_2,\varphi_2^*)$ is the first coefficient in the Fourier series expansion of the nonlinear function of damping $f(w,\dot{w})$. It is shown in Appendix A that $a_1(\varphi_2,\varphi_2^*)$ takes the following functional form:

$$a_1(\varphi_2,\varphi_2^*)=\varphi_2F(|\varphi_2|^2) \tag{6}$$

Therefore, Eq. (5) reads

$$\dot{\varphi}_1+\frac{\mathrm{i}\varepsilon}{2(1+\varepsilon)}(\varphi_1-\varphi_2)=\frac{\varepsilon A}{2}\exp(\mathrm{i}\varepsilon\sigma t)$$

$$\dot{\varphi}_2+\frac{\mathrm{i}\varepsilon}{2(1+\varepsilon)}(\varphi_2-\varphi_1)+(1+\varepsilon)\varphi_2F(|\varphi_2|^2)-\frac{\mathrm{i}(1+\varepsilon)}{2}|\varphi_2|^2\varphi_2=\frac{\varepsilon A}{2}\exp(\mathrm{i}\varepsilon\sigma t) \tag{7}$$

Let us define new variables

$$\tilde{\varphi}_j=\varphi_j\exp(-\mathrm{i}\varepsilon\sigma t),\quad j=1,2 \tag{8}$$

and substitute into Eq. (7). This system is transformed to the autonomous form:

$$\dot{\tilde{\varphi}}_1+\mathrm{i}\varepsilon\sigma\tilde{\varphi}_1+\frac{\mathrm{i}\varepsilon}{2(1+\varepsilon)}(\tilde{\varphi}_1-\tilde{\varphi}_2)=\frac{\varepsilon A}{2}$$

$$\dot{\tilde{\varphi}}_2+\mathrm{i}\varepsilon\sigma\tilde{\varphi}_2+\frac{\mathrm{i}}{2(1+\varepsilon)}(\tilde{\varphi}_2-\tilde{\varphi}_1)+(1+\varepsilon)\tilde{\varphi}_2F(|\tilde{\varphi}_2|^2)-\frac{\mathrm{i}(1+\varepsilon)}{2}|\tilde{\varphi}_2|^2\tilde{\varphi}_2=\frac{\varepsilon A}{2} \tag{9}$$

For the sake of brevity, the tilde mark appearing in Eq. (9) is omitted in further analysis. The fixed points of Eq. (9) (corresponding to periodic response regimes of the initial system) are solutions of the following set of algebraic equations:

$$\mathrm{i}\varepsilon\sigma\varphi_{10}+\frac{\mathrm{i}\varepsilon}{2(1+\varepsilon)}(\varphi_{10}-\varphi_{20})=\frac{\varepsilon A}{2}$$

$$\mathrm{i}\varepsilon\sigma\varphi_{20}+\frac{\mathrm{i}}{2(1+\varepsilon)}(\varphi_{20}-\varphi_{10})+(1+\varepsilon)\varphi_{20}F(|\varphi_{20}|^2)-\frac{\mathrm{i}(1+\varepsilon)}{2}|\varphi_{20}|^2\varphi_{20}=\frac{\varepsilon A}{2} \tag{10}$$

From Eq. (10), one easily obtains the algebraic equation with respect to a single complex variable:

$$G(|\varphi_{20}|^2)\varphi_{20}=\frac{(2\varepsilon\sigma+1)A}{4\sigma(1+\varepsilon)+2} \tag{11}$$

Taking the complex conjugate of Eq. (11) yields the additional equation:

$$G^*(|\varphi_{20}|^2)\varphi_{20}^*=\frac{(2\varepsilon\sigma+1)A}{4\sigma(1+\varepsilon)+2} \tag{12}$$

where

$$G=\mathrm{i}\left(\frac{2\varepsilon\sigma^2+\sigma}{2\sigma(1+\varepsilon)+1}-\frac{|\varphi_{20}|^2}{2}\right)+F(|\varphi_{20}|^2).$$

Multiplying Eq. (11) by φ_{20}^* and Eq. (12) by φ_{20}, and then multiplying the two equations, one obtains

$$G(|\varphi_{20}|^2)G^*(|\varphi_{20}|^2)|\varphi_{20}|^4=\frac{(2\varepsilon\sigma+1)^2A^2}{(4\sigma(1+\varepsilon)+2)^2}|\varphi_{20}|^2 \tag{13}$$

Canceling $|\varphi_{20}|^2$ from both sides of Eq. (13) yields

$$G(|\varphi_{20}|^2)G^*(|\varphi_{20}|^2)|\varphi_{20}|^2 = \frac{(2\varepsilon\sigma+1)^2A^2}{(4\sigma(1+\varepsilon)+2)^2} \tag{14}$$

Eq. (14) contains a single variable and should be solved for a specific shape of function G. Stability analysis of the periodic regimes is straightforward (linearization of Eq. (7) around a given fixed point). For a particular case of interest, this will be carried out in Section 3.

Previous studies [22–28] of similar systems have revealed the possibility for an alternative type of response in the vicinity of 1:1 resonance, referred to as a strongly modulated response (SMR). In the present section, we aim to extend the analytical description of the SMR presented earlier [26] to systems containing nonlinear damping in the general form. As demonstrated in previous studies [22–28], the SMR is characterized by abrupt changes in the amplitude of modulation of the response. The modulation profile consists of an interchange of "slow" and "super-slow" evolution peculiar to the relaxation type of motion [29–32].

Two time scales ("slow" and "super-slow") in the averaged Eq. (9) are introduced as follows: $\tau_0 = t$, $\tau_1 = \varepsilon t$. Formally, the "slow" time scale is the same as fast oscillations of the initial system; the term "slow" in this case reflects the rate of evolution of the averaged amplitudes without explicit definition of additional small parameters. The "slow" system evolves on the fast time scale $\tau_0 = t$, and in the leading approximation ($\varepsilon \to 0$) reads

$$\dot{\varphi}_1 = 0$$

$$\dot{\varphi}_2 + \frac{\mathrm{i}}{2}(\varphi_2 - \varphi_1) + \varphi_2 F(|\varphi_2|^2) - \frac{\mathrm{i}}{2}|\varphi_2|^2\varphi_2 = 0 \tag{15}$$

Therefore, in the leading approximation of slow system evolution, the variable φ_1 may be considered as constant because it comes from the first equation of Eq. (15). Therefore, $\varphi_1(\tau_1)$ depends only on time scale τ_1. However, the variable φ_2 evolves on the slow time scale τ_0. The fixed points of the second equation of Eq. (15) (denoted by Φ_1, Φ_2) depend only on the super-slow time scale τ_1 ($\Phi_1 = \Phi_1(\tau_1), \Phi_2 = \Phi_2(\tau_1)$) and obey the algebraic equation:

$$\frac{\mathrm{i}}{2}(\Phi_2 - \Phi_1) + \Phi_2 F(|\Phi_2|^2) - \frac{\mathrm{i}}{2}|\Phi_2|^2\Phi_2 = 0 \tag{16}$$

The algebraic relation given by Eq. (16) describes a super-slow invariant manifold (SIM) in four-dimensional state space. For better visualization of the SIM structure, we derive the projection of Eq. (16) on the $((|\Phi_2|, |\Phi_1|))$ plane. By simple algebraic manipulations, one obtains

$$|\Phi_2|^2((1-|\Phi_2|^2)^2 + 4F(|\Phi_2|^2)^2) = |\Phi_1|^2 \tag{17}$$

It is quite obvious that the topological shape of the projection curve defined by Eq. (17) is governed by $F(|\Phi_2|^2)$, which depends on characteristics of the nonlinear damping.

The next step is investigation of super-slow evolution of the flow at the SIM. Introducing the super-slow time scale $\tau_1 = \varepsilon t$ into Eq. (9) and considering the leading approximation ($\varepsilon \to 0$), one obtains the following system ($\varphi_1 = \Phi_1(\tau_1)$, $\varphi_2 = \Phi_2(\tau_1)$):

$$\Phi_1' + \mathrm{i}\sigma\Phi_1 + \frac{\mathrm{i}}{2}(\Phi_1 - \Phi_2) = \frac{A}{2}$$

$$\frac{\mathrm{i}}{2}(\Phi_2 - \Phi_1) + \Phi_2 F(|\Phi_2|^2) - \frac{\mathrm{i}}{2}|\Phi_2|^2\Phi_2 = 0 \tag{18}$$

The apostrophe denotes differentiation with respect to the super-slow time. The system given by Eq. (18) may be reduced to single complex equation:

$$\Phi_2' R(|\Phi_2|^2) - \Phi_2'^* H(\Phi_2, \Phi_2^*) = J(\Phi_2, \Phi_2^*)$$

$$R = 1 - 2\mathrm{i}F(|\Phi_2|^2) - 2\mathrm{i}\Phi_2 F_{\Phi_2}(|\Phi_2|^2) - 2|\Phi_2|^2$$

$$H = 2i\Phi_2 F_{\Phi_2^*}(|\Phi_2|^2) + \Phi_2^2$$

$$J = \frac{A}{2} - (1+2\sigma)F(|\Phi_2|^2)\Phi_2 + \frac{i}{2}|\Phi_2|^2\Phi_2(1+2\sigma) - i\sigma\Phi_2 \tag{19}$$

Up to this point, the treatment has been general. Further analysis is possible if the specific nonlinear damping function is known. In the next section, we analyze the case of piecewise-quadratic damping.

3. Piecewise-quadratic damping

3.1. Model

Quadratic damping characteristics given by

$$f = \lambda\dot{X}|\dot{X}| \tag{20}$$

are often considered for hydraulic damping devices [33] that are based on a flow of fluid through orifices in a moving piston. We consider piecewise-quadratic damping characteristics given by

$$f = \begin{cases} \lambda_1\dot{X}|\dot{X}|, & X < a_{cr} \\ \lambda_2\dot{X}|\dot{X}|, & X > a_{cr} \\ \lambda_2 > \lambda_1 \end{cases} \tag{21}$$

This type of damping characteristics is feasible in hydraulic dampers based on the same principle of orifice flow with the addition of semi-active control [34]. Such damping can be realized in hydraulic dampers containing several on/off orifice valves in a moving piston. Such a design is somewhat different from the dampers considered in Ref. [34] for which the on/off orifice valves were installed outside the chamber of the damper. During its motion, once the piston reaches some critical value of deflection (defined by the designer), a_{cr}, some of the orifices are closed and thus the damping coefficient increases. When the piston hits the critical value a_{cr} in the opposite direction, it simply reopens the closed orifices, thus bringing the damping coefficient to its original value λ_1. A schematic example of such a damper is presented in Fig. 1.

Since the number of piston orifices and on/off orifice valves (as well as their diameter) may be varied, there is certain flexibility in the choice of λ_1, λ_2 parameters. However, precise implementation of such a damper is beyond the scope of the paper.

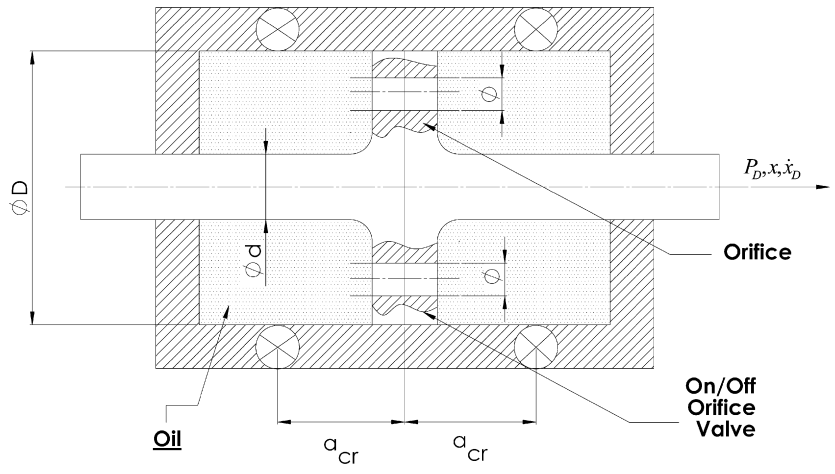

Fig. 1. Semi-active on–off orifice viscous fluid damper (concept).

3.2. Analytical treatment

The system under investigation is described by the following nonlinear damping characteristics:

$$f=\begin{cases}\lambda_1(\dot{y}_1-\dot{y}_2)|(\dot{y}_1-\dot{y}_2)|, & |y_1-y_2|<a_{cr}\\ \lambda_2(\dot{y}_1-\dot{y}_2)|(\dot{y}_1-\dot{y}_2)|, & |y_1-y_2|>a_{cr}\\ \lambda_2>\lambda_1\end{cases} \tag{22}$$

We begin the analytical study from a description of the periodic regimes of the system containing nonlinear damping characteristics as given by Eq. (22), including stability analysis. Thus, from Eqs. (2)–(5), with the damping function described by Eq. (22), the following averaged system (in a vicinity of 1:1 resonance) is obtained:

$$\dot{\varphi}_1+\frac{\mathrm{i}\varepsilon}{2(1+\varepsilon)}(\varphi_1-\varphi_2)=\frac{\varepsilon A}{2}\exp(\mathrm{i}\varepsilon\sigma t)$$

$$\dot{\varphi}_2+\frac{\mathrm{i}\varepsilon}{2(1+\varepsilon)}(\varphi_2-\varphi_1)+(1+\varepsilon)a_1-\frac{\mathrm{i}(1+\varepsilon)}{2}|\varphi_2|^2\varphi_2=\frac{\varepsilon A}{2}\exp(\mathrm{i}\varepsilon\sigma t)$$

$$a_1=\begin{cases}\dfrac{4\lambda_1\varphi_2|\varphi_2|}{3\pi}, & |\varphi_2|<a_{cr}\\ \dfrac{\varphi_2}{\pi}\left(2(\lambda_1-\lambda_2)\left(a_{cr}-\dfrac{a_{cr}^3}{3|\varphi_2|^2}\right)+\dfrac{4}{3}\lambda_2|\varphi_2|\right), & |\varphi_2|>a_{cr}\end{cases} \tag{23}$$

Therefore,

$$F=\begin{cases}\dfrac{4\lambda_1|\varphi_2|}{3\pi}, & |\varphi_2|<a_{cr}\\ \dfrac{1}{\pi}\left(2(\lambda_1-\lambda_2)\left(a-\dfrac{a^3}{3|\varphi_2|^2}\right)+\dfrac{4}{3}\lambda_2|\varphi_2|\right), & |\varphi_2|>a_{cr}\end{cases} \tag{24}$$

Writing Eq. (23) in an autonomous form according to Eq. (10), one obtains

$$\dot{\varphi}_1+\mathrm{i}\varepsilon\sigma\varphi_1+\frac{\mathrm{i}\varepsilon}{2(1+\varepsilon)}(\varphi_1-\varphi_2)=\frac{\varepsilon A}{2}$$

$$\dot{\varphi}_2+\mathrm{i}\varepsilon\sigma\varphi_2+\frac{\mathrm{i}}{2(1+\varepsilon)}(\varphi_2-\varphi_1)+(1+\varepsilon)\varphi_2F(|\varphi_2|^2)-\frac{\mathrm{i}(1+\varepsilon)}{2}|\varphi_2|^2\varphi_2=\frac{\varepsilon A}{2} \tag{25}$$

3.2.1. Periodic responses

Applying Eq. (14) for the piecewise-quadratic damping case, one obtains the following algebraic equations related to system periodic responses:

$$G^{(1)}G^{(1)^*}|\varphi_{20}|^2=\frac{(2\varepsilon\sigma+1)^2A^2}{(4\sigma(1+\varepsilon)+2)^2}, \quad |\varphi_2|<a_{cr}$$

$$G^{(2)}G^{(2)^*}|\varphi_{20}|^2=\frac{(2\varepsilon\sigma+1)^2A^2}{(4\sigma(1+\varepsilon)+2)^2}, \quad |\varphi_2|>a_{cr} \tag{26}$$

where

$$G^{(1)}=\mathrm{i}\left(\frac{2\varepsilon\sigma^2+\sigma}{2\sigma(1+\varepsilon)+1}-\frac{|\varphi_{20}|^2}{2}\right)+F^{(1)}, \quad G^{(2)}=\mathrm{i}\left(\frac{2\varepsilon\sigma^2+\sigma}{2\sigma(1+\varepsilon)+1}-\frac{|\varphi_{20}|^2}{2}\right)+F^{(2)}$$

In order to study the stability of the periodic response regimes, we develop variation equations near fixed points determined by Eq. (14). For the sake of convenience, the term $|\varphi_2|$ appearing in Eq. (24) is rewritten as follows:

$$|\varphi_2| = \sqrt{\varphi_2\varphi_2^*} \tag{27}$$

Substituting Eq. (27) into Eq. (24), one obtains

$$F = \begin{cases} \dfrac{4\lambda_1\sqrt{\varphi_2\varphi_2^*}}{3\pi}, & |\varphi_2| < a_{cr} \\ \dfrac{1}{\pi}\left(2(\lambda_1-\lambda_2)\left(a - \dfrac{a^3}{3\varphi_2\varphi_2^*}\right) + \dfrac{4}{3}\lambda_2\sqrt{\varphi_2\varphi_2^*}\right), & |\varphi_2| > a_{cr} \end{cases}$$

Small perturbations around the fixed points of Eq. (25) (denoted by $\varphi_{10}, \varphi_{20}$) are considered as follows:

$$\varphi_1 = \varphi_{10} + \delta_1; \quad \varphi_2 = \varphi_{20} + \delta_2 \tag{28}$$

Linear perturbation equations near the fixed points $\varphi_{10}, \varphi_{20}$ are

$$\dot{\delta}_1 + \mathrm{i}\varepsilon\sigma\delta_1 + \frac{\mathrm{i}\varepsilon}{2(1+\varepsilon)}(\delta_1 - \delta_2) = \frac{\varepsilon A}{2}$$

$$\dot{\delta}_1^* + \mathrm{i}\varepsilon\sigma\delta_1^* - \frac{\mathrm{i}\varepsilon}{2(1+\varepsilon)}(\delta_1^* - \delta_2^*) = \frac{\varepsilon A}{2}$$

$$\begin{aligned} &\dot{\delta}_2 + \mathrm{i}\varepsilon\sigma\delta_2 + \frac{\mathrm{i}}{2(1+\varepsilon)}(\delta_2 - \delta_1) + (1+\varepsilon)\delta_2 F(\varphi_{20}, \varphi_{20}^*) \\ &\quad + (1+\varepsilon)\varphi_{20}\left\{\left.\frac{\partial F}{\partial\varphi_2}\right|_{\varphi_{20},\varphi_{20}^*}\delta_2 + \left.\frac{\partial F}{\partial\varphi_2^*}\right|_{\varphi_{20},\varphi_{20}^*}\delta_2^*\right\} - \mathrm{i}(1+\varepsilon)|\varphi_{20}|^2\delta_2 - \frac{\mathrm{i}(1+\varepsilon)}{2}\varphi_{20}^2\delta_2^* = \frac{\varepsilon A}{2} \\ &\dot{\delta}_2^* - \mathrm{i}\varepsilon\sigma\delta_2^* - \frac{\mathrm{i}}{2(1+\varepsilon)}(\delta_2^* - \delta_1^*) + (1+\varepsilon)\delta_2^* F(\varphi_{20}, \varphi_{20}^*) \\ &\quad + (1+\varepsilon)\varphi_{20}^*\left\{\left.\frac{\partial F}{\partial\varphi_2}\right|_{\varphi_{20},\varphi_{20}^*}\delta_2^* + \left.\frac{\partial F}{\partial\varphi_2^*}\right|_{\varphi_{20},\varphi_{20}^*}\delta_2\right\} + \mathrm{i}(1+\varepsilon)|\varphi_{20}|^2\delta_2^* + \frac{\mathrm{i}(1+\varepsilon)}{2}\varphi_{20}^*\delta_2^* = \frac{\varepsilon A}{2} \end{aligned} \tag{29}$$

This system of equations should be solved separately for two domains of the damping function $F^{(1)}$ and $F^{(2)}$ depending on the particular value of $|\varphi_2|$. Asymptotic stability of the periodic responses is determined by the eigenvalues of the Jacobian of the linear system (29). As one would expect, generic Hopf and saddle-node bifurcations were observed, and these are marked on the frequency-response diagrams (describing the amplitude of φ_2 as a function of frequency detuning) by "H" and "SN", respectively (Figs. 2a and b).

3.2.2. *Strongly modulated response (SMR)*

We proceed with construction of the SIM projection (on the $(|\Phi_1|, |\Phi_2|)$ plane) using Eq. (17). Contrary to the previously studied cases where the damping coefficient $F(|\varphi_2|^2)$ was uniform (the same functional expression), for the piecewise-quadratic damping case, $F(|\varphi_2|^2)$ changes its functional expression when $|\varphi_2|$ crosses the critical threshold value a_{cr}. Consequently, we should consider this change when describing the SIM approximation and mechanism of relaxation. Constructing the SIM projection, we apply Eq. (17) separately for each interval of $|\varphi_2|$. Thus, drawing the SIM projection for the interval $|\varphi_2| < a_{cr}$ we have:

$$|\Phi_2|^2((1-|\Phi_2|^2)^2 + 4F^{(1)}(|\Phi_2|^2)^2) = |\Phi_1|^2 \tag{30}$$

Similarly, for the interval $|\varphi_2| > a_{cr}$:

$$|\Phi_2|^2((1-|\Phi_2|^2)^2 + 4F^{(2)}(|\Phi_2|^2)^2) = |\Phi_1|^2 \tag{31}$$

where $F^{(1)}$ and $F^{(2)}$ are determined in Eq. (24).

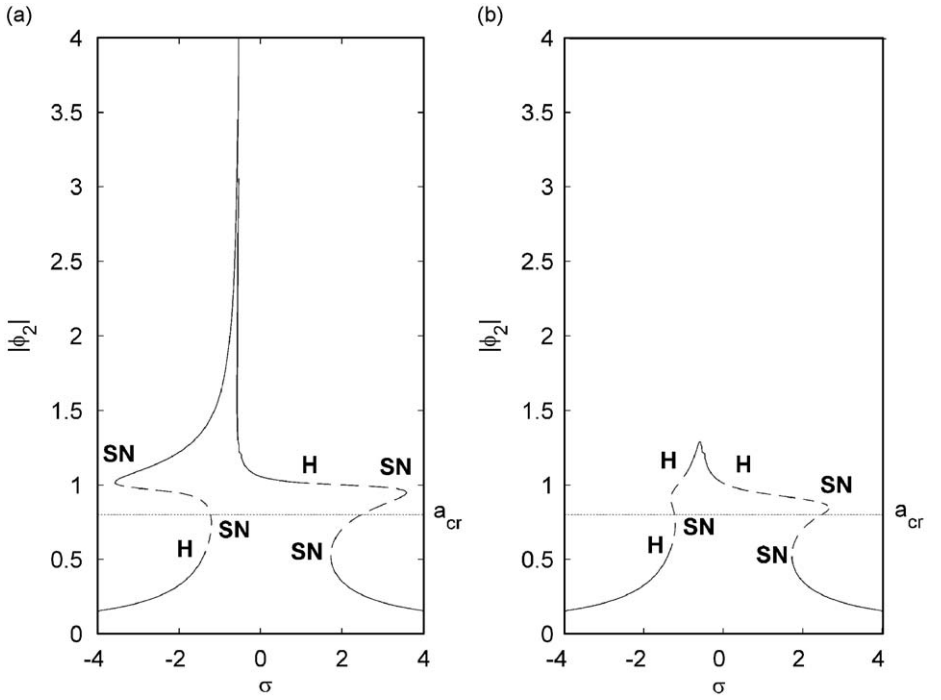

Fig. 2. Frequency-response curves: (a) quadratic damping case ($A = 1.2$, $\lambda_1 = \lambda_2 = 0.2$, $\varepsilon = 0.01$, $a_{cr} = 0.8$) and (b) piecewise-quadratic damping case ($A = 1.2$, $\lambda_1 = 0.2$, $\lambda_2 = 6$, $\varepsilon = 0.01$, $a_{cr} = 0.8$). Solid lines refer to stable solutions where dashed lines refer to unstable ones.

To illustrate the SIM projections for the discussed case of piecewise-quadratic damping, we fix the values of λ_1 and a_{cr}, varying the values of λ_2 only. In Fig. 3, we plot the SIM projections for two distinct values of a_{cr} ($a_{cr} = 0.8$, $a_{cr} = 1.1$).

One of the SIM curves presented in both plots of Fig. 3 refers to the case of pure quadratic damping ($\lambda_2 = \lambda_1$). As observed in both diagrams of Fig. 3, as λ_2 grows, all SIM curves bend more and more towards the critical value (a_{cr}, marked with the vertical dashed line on the diagrams). Therefore, despite the increase of one of the damping components, it is possible (by the appropriate choice of a_{cr}) to preserve the SIM projection curve in a folded form necessary for relaxation oscillations (the SMR). In order to keep the SIM projection curve folded, a_{cr} should be picked above the lower fold of the curve.

In order to describe the super-slow evolution of the system on the stable branches of the SIM, we refer to Eq. (19). Splitting into modulus and argument, $\Phi_2 = N(\tau_1)\exp(\mathrm{i}\theta(\tau_1))$, one obtains a 2-dof reduced flow system in polar coordinates. If $N < a_{cr}$ the super-slow system reads

$$F = \frac{4\lambda_1 N}{3\pi},$$

$$a_{11} = 1 - 3N^2, \quad a_{12} = 2NF, \quad a_{21} = -2\left(F + \frac{\mathrm{d}F}{\mathrm{d}N}N\right), \quad a_{22} = N - N^3$$

$$f_1 = -(2\sigma + 1)FN + \frac{A}{2}\cos\theta;$$

$$f_2 = \left(\sigma + \frac{1}{2}\right)(N^3 - N) + \frac{N}{2} - \frac{A}{2}\sin\theta$$

$$N' = \frac{f_1 a_{22} - f_2 a_{12}}{a_{11}a_{22} - a_{12}a_{21}}; \quad \theta' = \frac{f_2 a_{11} - f_1 a_{21}}{a_{11}a_{22} - a_{12}a_{21}} \tag{32a}$$

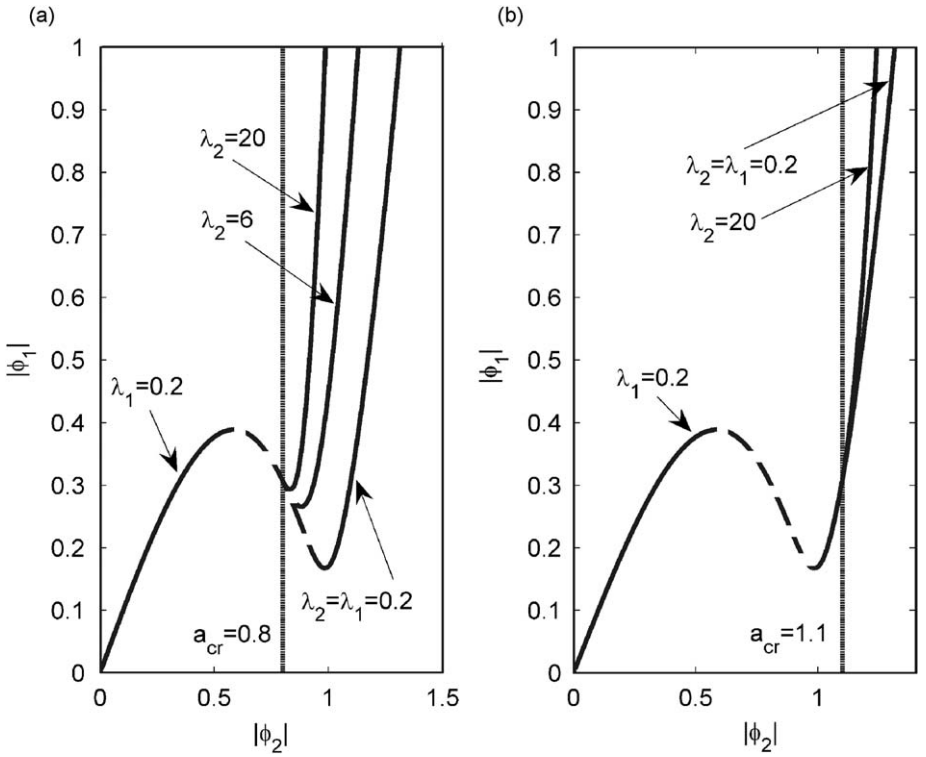

Fig. 3. SIM projections: (a) $\lambda_1 = 0.2$, $a_{cr} = 0.8$, $\lambda_2 = 0.2$, 6, 20 and (b) $\lambda_1 = 0.2$, $a_{cr} = 1.1$, $\lambda_2 = 0.2$, 20. Solid lines refer to stable branches of SIM when the dashed lines refer to unstable ones.

If $N > a_{cr}$, the super-slow system reads

$$F = \frac{1}{\pi}\left(2(\lambda_1 - \lambda_2)\left(a_{cr} - \frac{a_{cr}^3}{3N^2}\right) + \frac{4}{3}\lambda_2 N\right),$$

$$a_{11} = 1 - 3N^2, \quad a_{12} = 2NF, \quad a_{21} = -2\left(F + \frac{\mathrm{d}F}{\mathrm{d}N}N\right), \quad a_{22} = N - N^3$$

$$f_1 = -(2\sigma + 1)FN + \frac{A}{2}\cos\theta;$$

$$f_2 = \left(\sigma + \frac{1}{2}\right)(N^3 - N) + \frac{N}{2} - \frac{A}{2}\sin\theta$$

$$N' = \frac{f_1 a_{22} - f_2 a_{12}}{a_{11}a_{22} - a_{12}a_{21}}; \quad \theta' = \frac{f_2 a_{11} - f_1 a_{21}}{a_{11}a_{22} - a_{12}a_{21}} \tag{32b}$$

Denoting the numerators and denominator of the right-hand side of system given by Eq. (32) by $f_1(N,\theta)$ for the first equation, $f_2(N,\theta)$ for the second equation, and $g(N)$ for the denominator, the system of Eqs. (32a) and (32b) is presented in the following form:

$$\frac{\partial N}{\partial \tau} = \frac{f_1(N,\theta)}{g(N)}$$

$$\frac{\partial \theta}{\partial \tau} = \frac{f_2(N,\theta)}{g(N)} \tag{33}$$

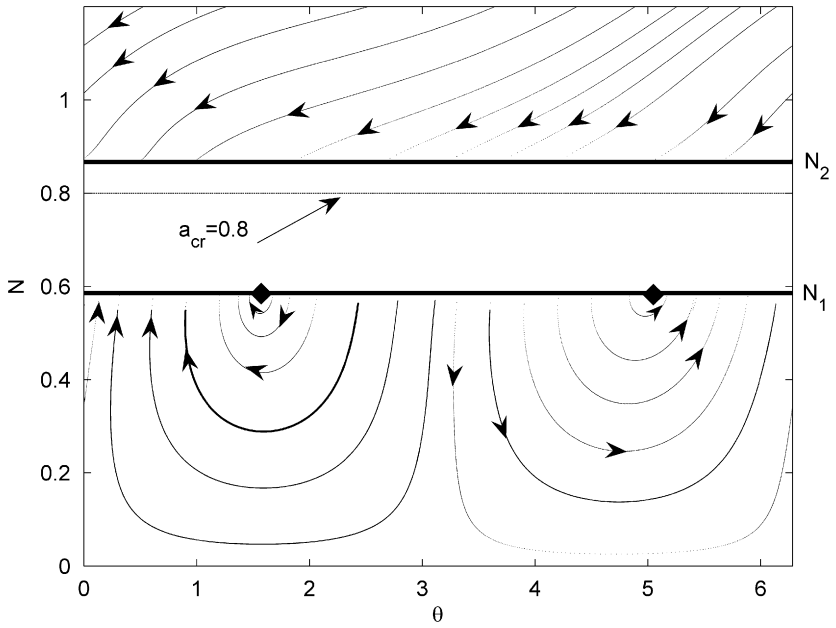

Fig. 4. Phase portrait. System parameters are ($\lambda_1 = 0.2,\ \lambda_2 = 8,\ a_{cr} = 0.8,\ \sigma = 0,\ A = 0.5$). Diamonds on the fold lines refer to the folded singularities.

Rescaling time by the function $g(N)$ yields the super-slow flow equations:

$$N' = f_1(N, \theta)$$

$$\theta' = f_2(N, \theta) \tag{34}$$

The phase portrait of the system given by Eqs. (32a) and (32b) is presented in Fig. 4 (system parameters: $\lambda_1 = 0.2,\ \lambda_2 = 6, a_{cr} = 0.8,\ \sigma = 0,\ A = 0.5$). Fold curves N_1, N_2 are marked on the phase portrait as bold lines.

Observing the phase portrait presented on Fig. 4, one can identify the pair of folded foci on the lower fold. These folded singularities are denoted by diamonds on the figure. There are no other fixed points for this particular set of system parameters. An additional peculiarity of the phase portrait that should be noted is the existence of trajectories that end at the fold lines on both stable branches of the SIM. As was demonstrated earlier [23,24,26], this fact suggests the possible existence of relaxation type motion or the SMR. In order to determine the existence of the SMR, we construct one-dimensional mapping diagrams in a manner described in Ref. [26]. In describing the process of one-dimensional mapping diagram construction, we will briefly repeat the analysis carried out in Ref. [26].

From the phase portrait presented in Fig. 4, we can see that there is an interval of θ (on the lower fold line N_1) for which all phase trajectories can arrive to and jump from N_1. This interval is bounded by the folded singularities (for the case illustrated on Fig. 4, these folded singularities are stable foci marked with diamonds on the figure). We denote this interval by $R = [\Theta_1, \Theta_2]$, where Θ_1, Θ_2 are the folded singularities that constitute the boundaries of the jump interval. In the regime of the relaxation oscillations, the phase trajectory jumps from a point of this interval to the upper branch of the SIM, then it moves along the line of the super-slow flow to the upper fold line, then jumps back to the lower branch and moves to the lower fold line, commencing on one of the points of the interval R in order to enable the next jump. Therefore, it is natural to consider this regime as a mapping of the interval R into itself—the regime of the relaxation oscillations will correspond to attractor of this one-dimensional map. The existence of this attractor is therefore a necessary and sufficient condition for existence of the SMR for the system given by Eq. (3.3) when the mass ratio ε is small enough.

In order to construct the relevant map, we should separately consider the "super-slow" and the "slow" parts of the mapping cycle. As for the "super-slow" parts on the lower and the upper branches of the SIM, we can use Eqs. (32a) and (32b) and directly connect the "entrance" and "exit" points by numeric integration. As for the "slow" parts, the function φ_2 should be continuous at the points of contact between the "slow" and the "super-slow" parts. Therefore, for the "slow" parts of the motion, one exploits the complex invariant $\Phi_1(\tau)$, which can be expressed by Eq. (16), providing

$$\Phi_2 - 2i\Phi_2 F(|\Phi_2|^2) - |\Phi_2|^2\Phi_2 = \Phi_1(\tau_1) \tag{35}$$

where F is given by Eq. (24).

If one knows its value at the point of the "jump" at the fold line, it is possible to compute N and θ for the point of "finish" unambiguously and thus to complete the mapping. Let us denote the point of finish by (N_x, θ_x) and the start point on the jump interval R as (N_0, θ_0) ($N_0 = N_1$, since the jump interval belongs to the lower fold N_1). Contrary to the previously considered cases [22–28] (linear damping), we deal here with the piecewise-quadratic damping case. Therefore, a_{cr} may be situated between the folds (N_1, N_2) (see Fig. 3a, for example). Therefore, the jump from one stable branch to another results in crossing a_{cr}, causing the function F to change its form. This case is illustrated in Fig. 3a. In this case, the function describing the upper stable branch of SIM is rather complicated, and therefore we cannot derive the closed form solution for N_x, θ_x. In order to make the analysis of jumps more clear, we present the algorithm for calculation of the N_x, θ_x pair for two values of a_{cr}, namely $N_1 < a_{cr} < N_2$, $N_2 < a_{cr}$ (Appendix B).

Not every trajectory that starts from the lower fold of the SIM will reach the initial interval ($R = [\Theta_1,\ \Theta_2]$), since it can go to the alternative attractor at the upper or the lower branch of the SIM if it exists. Only those

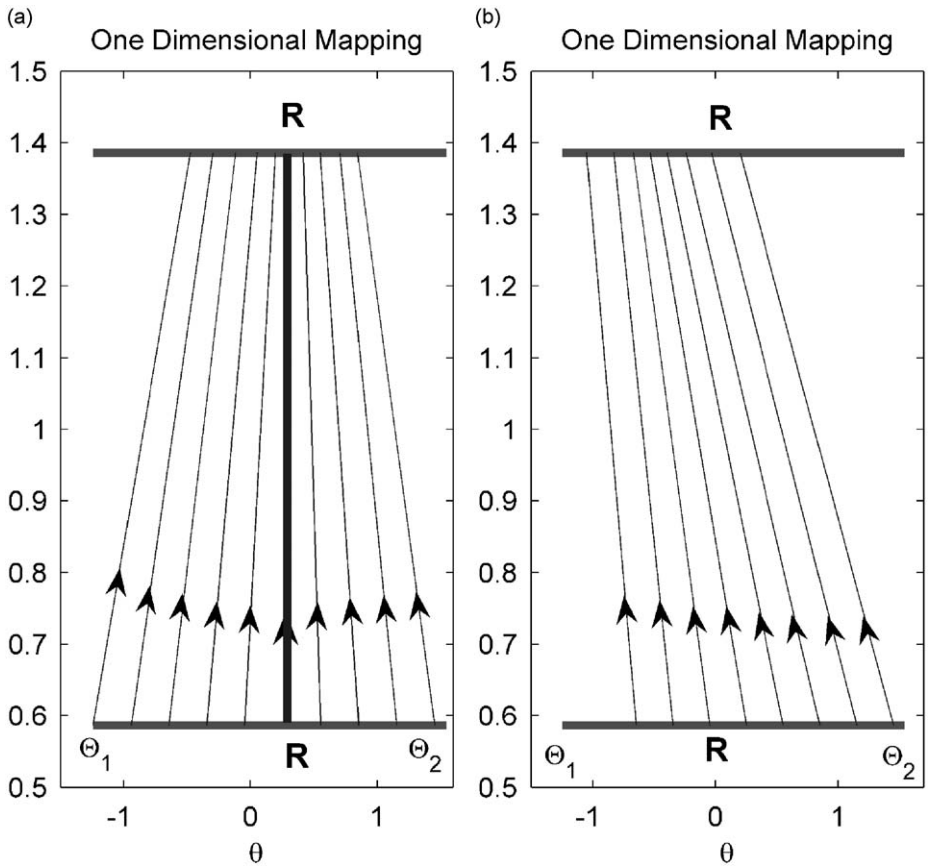

Fig. 5. One-dimensional return maps diagram: (a) $\sigma = 0$ and (b) $\sigma = 1$. Rest system parameters: $A = 0.5$, $\lambda_1 = 0.2$, $\lambda_2 = 8$, $a_{cr} = 0.8$. Bold line refers to the stable cycle of the map.

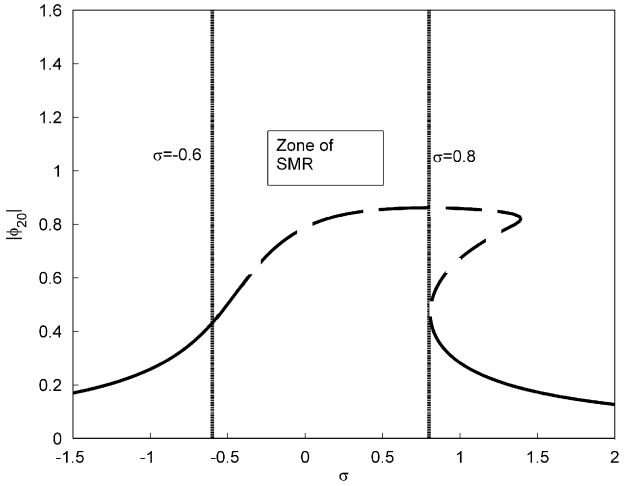

Fig. 6. Frequency-response diagram. Frequency-detuning interval for SMR existence is marked with thin dashed vertical lines. Bold curve refers to the periodic regimes solution. Bold dashed lines relate to the unstable solutions. System parameters: $A = 0.5$, $\lambda_1 = 0.2$, $\lambda_2 = 8$, $a_{cr} = 0.8$, $\varepsilon = 0.01$.

points that are mapped into the interval R can carry sustained relaxation oscillations. To illustrate this, two return maps were constructed for different values of frequency detuning ($\sigma = 0$, $\sigma = 1$) (see Fig. 5).

Fig. 5 depicts the resulting one-dimensional return map from R into R. Analyzing the results of Fig. 5, one can easily conclude that the map illustrated in Fig. 5a indicates the existence of the SMR response related to the stable cycle on the map (this cycle is marked with a bold line in Fig. 5a). The map of Fig. 5b contains no stable cycle, and therefore no SMR response exists in the system for $\sigma = 1$. Therefore, using these maps for various values of system parameters, one can determine the parametric zones of existence of the SMR by this semi-analytical procedure. The frequency-detuning interval for which SMR response exists is depicted below on the frequency-response curve (Fig. 6) for the same set of system parameters: $A = 0.5$, $\lambda_1 = 0.2$, $\lambda_2 = 8$, $a_{cr} = 0.8$, $\varepsilon = 0.01$.

4. Tuning of piecewise-quadratic damping to prevent undesired periodic regimes

4.1. Concept of tuning

As demonstrated in previous studies, attaching the NES to the main linear system subject to harmonic excitation may be a rather effective method for vibration mitigation. Apparently, existence of a cubic nonlinearity in the system may cause the appearance of additional branches of the undesired periodic responses, resulting in high amplitude excitations of the entire system. Thus, effective regimes may coexist with ineffective ones. Therefore, our goal is to preserve the effective regimes from the point of view of vibration suppression (e.g., SMR and the periodic regimes of the lower branch of the frequency-response curve), and at the same time, to eliminate the destructive ones.

To achieve this, we should obey the principles listed below for correct tuning of the piecewise damping:

1. Set up λ_2 to be essentially higher then λ_1 ($\lambda_2 > \lambda_1$). This can destroy the stable branches of the periodic regime that pertain to the high amplitude vibration regime (for the coordinate of the relative displacement $y_1 - y_2$). It will be demonstrated that, at these stable branches, not only does the relative displacement coordinate have a relatively large amplitude of vibration, but the main mass does also.
2. Set up a_{cr} in such a way to obtain periodic attractors only in the region below a_{cr}. Otherwise, high-amplitude periodic responses at the upper branch of the SIM will jeopardize the vibration suppression. In some cases, this is not possible, as will be discussed below.

3. The value of a_{cr} will be higher than the value of the lower fold of the SIM ($N_1 < a_{cr}$). This is necessary for the existence of the SMR. Otherwise, the system will have only periodic or quasiperiodic responses.

4.2. Drawbacks of linear and quadratic damping characteristics

We begin with an example with constant value of amplitude of excitation ($A = 0.4$).

As demonstrated earlier [23,24] for the case of linear damping characteristics, the necessary condition for the SMR response to exist is $0 < \lambda < 1/\sqrt{3}$ for arbitrary amplitude of excitation. Since the restriction on damping coefficient constitutes only the necessary condition, then for some values of the external forcing, this range can become smaller. It should be noted that gradually increasing the value of damping (up to $\lambda = 1/\sqrt{3}$) causes weakening of the undesired response; however, it also weakens the SMR response, making it less effective and less robust.

Choosing the values of $\lambda = 0.2$, 1, let us plot the frequency-response diagrams for the fixed value of the external forcing amplitude $A = 0.4$ (Fig. 7). The interval of the SMR existence is also marked.

Observing the frequency-response diagrams in Fig. 7, one can note that increasing the value of damping above some critical value in a range $\lambda_{cr} \leqslant 1/\sqrt{3}$ results in disappearance of the SMR. We can also observe the vanishing of the branch of undesired response. To illustrate this, we present the time series plot (Figs. 8a and b) (for the deflection of the main mass as a function of time) for $\lambda = 0.2$ and 1; the other parameters are $A = 0.4$, $\sigma = 0$, $\varepsilon = 0.01$.

The results presented in Fig. 8 demonstrate that the SMR response is better for vibration suppression than the simple periodic regime obtained for the same set of system parameters, but for the increased value of damping. Effectiveness of the SMR regime becomes more visible with the growth of the external forcing

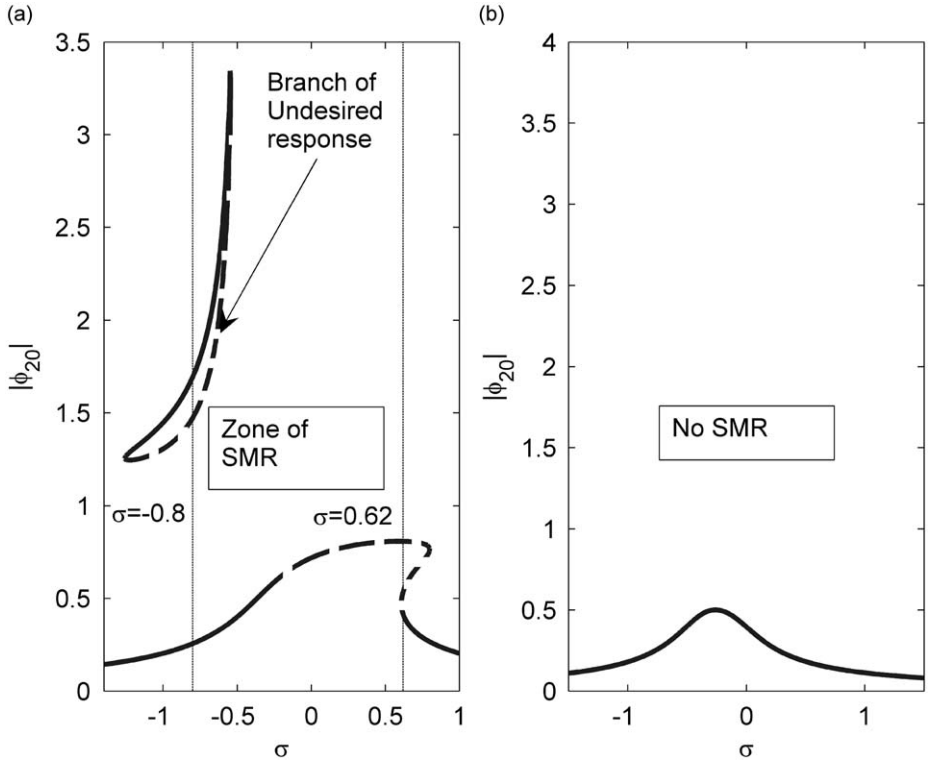

Fig. 7. Frequency-response diagram for a linear damping case. Frequency-detuning interval for the SMR existence is marked with thin dashed vertical lines. Bold curve refers to the periodic regimes solution. Bold dashed lines relate to the unstable solutions: (a) $\lambda = 0.2$ and (b) $\lambda = 1 > 1/\sqrt{3}$. Amplitude of excitation $A = 0.4$.

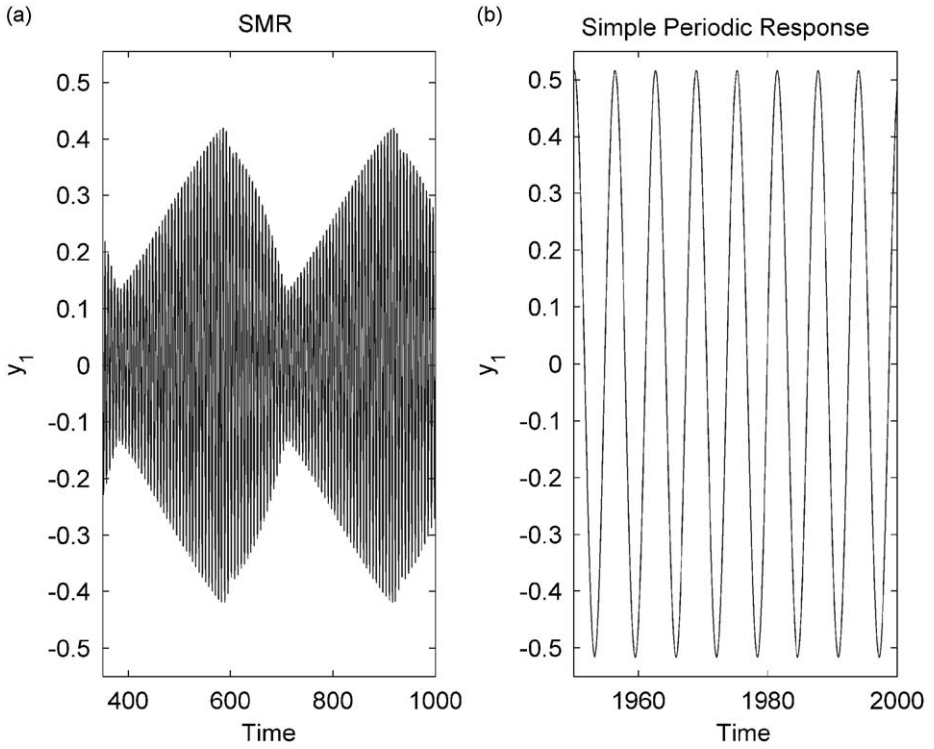

Fig. 8. Time series: (a) system vibrates in SMR regime for $\lambda = 0.2$ and (b) simple periodic response (no SMR exists) for $\lambda = 1$. System parameters: $A = 0.4$, $\sigma = 0$, $\varepsilon = 0.01$.

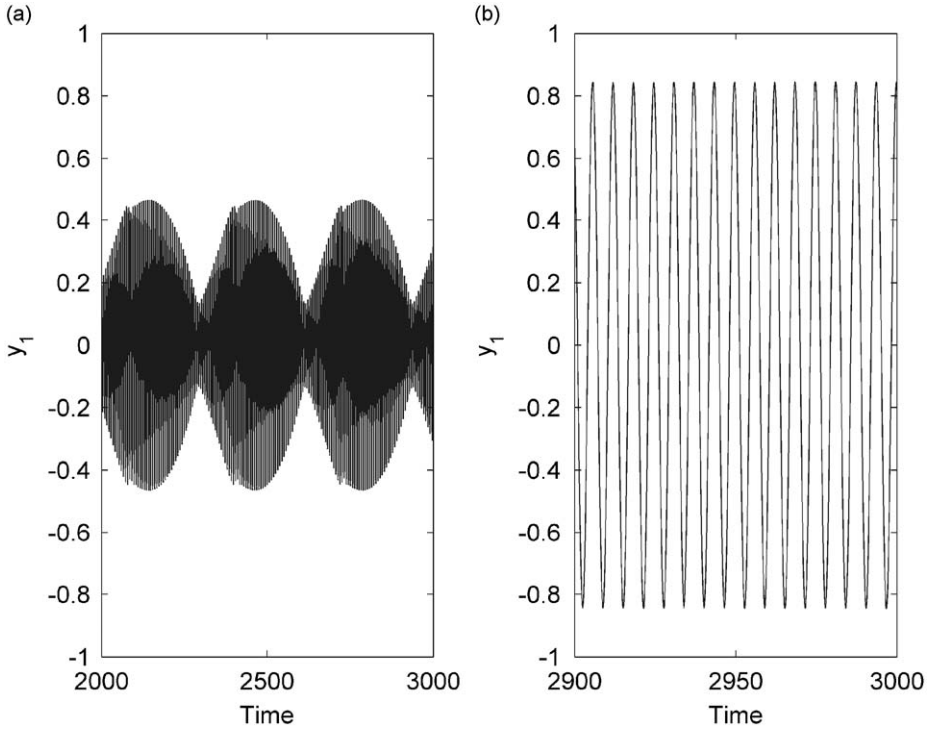

Fig. 9. Time series: (a) system vibrates in SMR regime for $\lambda = 0.2$ and (b) simple periodic response (no SMR exists) for $\lambda = 2.5$. System parameters: $A = 0.8$, $\sigma = 0$, $\varepsilon = 0.01$.

amplitude, as illustrated in Fig. 9 for $A = 0.8$ (the other parameters remain the same—$\sigma = 0$, $\varepsilon = 0.01$). The first damping coefficient was chosen to enable the existence of the SMR ($\lambda = 0.2$), while the second one was picked to eliminate the branch of undesired periodic regimes ($\lambda = 2.5$).

Observing the time series plots in Fig. 9, one also can note the preference for the SMR over the simple periodic response regime even for a relatively small value of the forcing amplitude. Therefore, summarizing the results, we conclude that, by increasing the damping coefficient, we can weaken and even totally annihilate the branch of the undesired response. However, the remaining periodic regimes become more and more inefficient (in a sense of vibration suppression) with the growing values of damping coefficient and also the amplitudes of excitation.

In the case of simple quadratic damping, the frequency-response curves are qualitatively the same and are not demonstrated here. When analyzing quadratic damping, one obtains the same result: for relatively small damping values, the branches of the undesired responses exist; however, increases in the damping coefficient cause elimination of the undesired branches together with the desired responses (e.g., the SMR). In the following subsection, we demonstrate the ability of piecewise-quadratic damping to preserve the robustness of the effective SMR response and totally annihilate the undesired branches.

4.3. Tuning the damper with piecewise-quadratic characteristics

Let us consider the same system parameters as in the example of the previous subsection ($A = 0.4$, $\lambda = 0.2$). As demonstrated in the previous section, we need to determine the coefficients of the piecewise-quadratic damping (λ_1, λ_2) as well as the a_{cr} value to eliminate the undesired periodic response and also to preserve the SMR response. Following the first principle of tuning listed in Section 4.1, we assign λ_1 the value of linear damping for which the SMR exists: $\lambda_1 = 0.2$ (see previous, Section 4.2). According to the same principle, we assign λ_2 a value that is much higher than λ_1 to obey ($\lambda_2 > \lambda_1$) $\lambda_2 = 8$. We set the value of a_{cr} according to

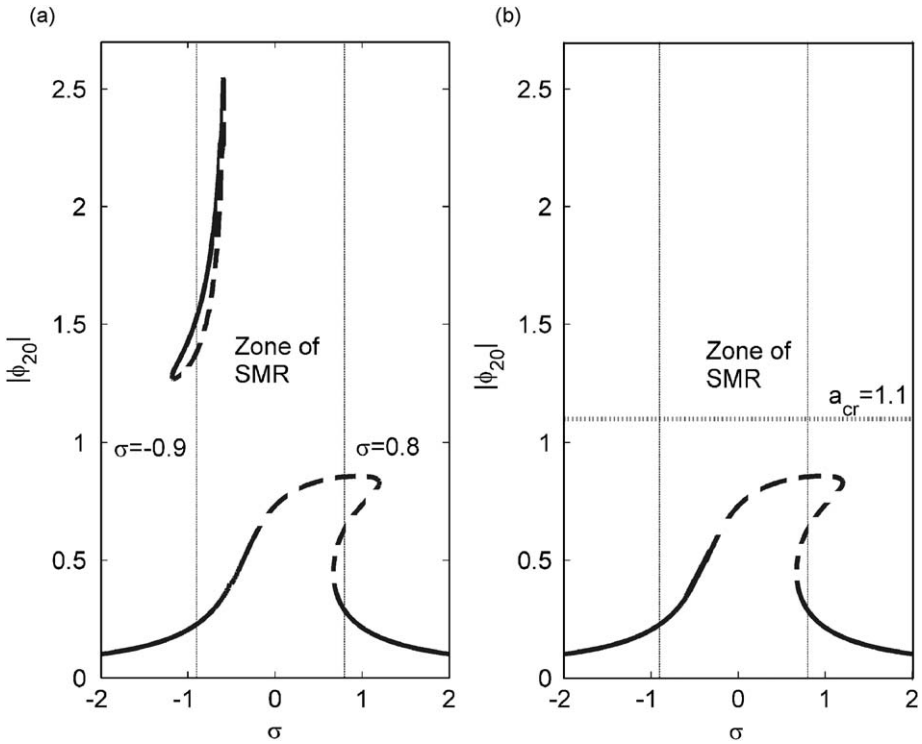

Fig. 10. Frequency-response diagrams: (a) quadratic damping case $\lambda_2 = \lambda_1 = 0.2$ and (b) piecewise-quadratic damping case $\lambda_2 = 6$; $\lambda_1 = 0.2$. Rest system parameters: $A = 0.4$, $\varepsilon = 0.01$.

principles 2 and 3. Therefore, the value of a_{cr} will be situated between the branch of the undesired periodic response and the lower branch of the periodic response to fulfill principle 2. Determination of a_{cr} also requires accounting for the third principle. Therefore, a_{cr} should also obey ($a_{cr} > N_1 = 0.595$). Satisfying the requirements of principles 2 and 3, we pick the value of a_{cr} to be $a_{cr} = 1.1$. We illustrate the results of tuning via the frequency-response plot (Figs. 10a and b). For pure quadratic damping ($\lambda_2 = \lambda_1 = 0.2$), this is plotted in Fig. 10a; for piecewise-quadratic damping ($\lambda_1 = 0.2$, $\lambda_2 = 8$) it is plotted in Fig. 10b. The interval of the SMR is also marked on both plots of Fig. 10.

Comparing the frequency-response diagram of the quadratic case to the piecewise-quadratic one, we note the absence of the branch of undesired periodic responses in the latter case. It is also clear from these diagrams that the frequency interval of the SMR existence is preserved. From the point of view of the tuning guidelines given in Section 4.1, all principles for proper tuning are obeyed, namely $\lambda_2 > \lambda_1$ and thus the first principle is fulfilled. Recommendation 2 is satisfied since there are no periodic attractors above the value of a_{cr}. Finally, recommendation 3 is satisfied since the value of a_{cr} has been picked as above the lower fold N_1, thus allowing relaxation type motion (SMR).

In the following figure, we plot the frequency-response diagrams for piecewise-quadratic damping coefficients tuned for various values of external forcing amplitudes.

It is clear from Figs. 11a–c, that, for the given values of external forcing amplitude ($A = 0.6, 0.8, 1$), piecewise-quadratic damping may be tuned to prevent undesired periodic responses and also to preserve the effective regimes. However, for increased values of the amplitude of excitation $A = 1.2 > 1$, as from the diagram of Fig. 11d, the second principle of tuning is violated. To understand the encountered problem of tuning for the case illustrated on Fig. 11d, we study the case of simple quadratic damping for the same value of

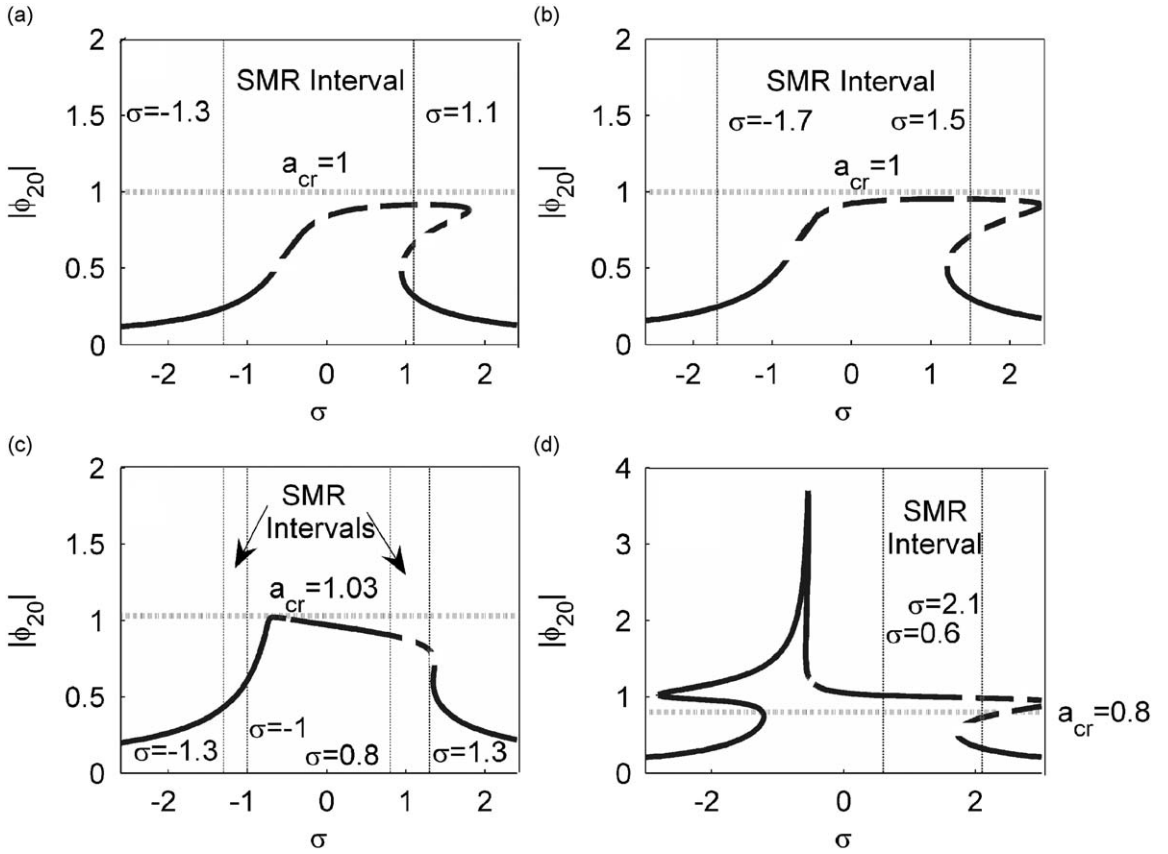

Fig. 11. Frequency-response diagrams: (a) $A = 0.6$, tuning parameters: $\lambda_1 = 0.2$, $\lambda_2 = 8$, $a_{cr} = 1$; (b) $A = 0.8$, tuning parameters: $\lambda_1 = 0.2$, $\lambda_2 = 8$, $a_{cr} = 1$; (c) $A = 1$, tuning parameters: $\lambda_1 = 0.5$, $\lambda_2 = 18$, $D : a_{cr} = 1.05$; and (d) $A = 1.2$, tuning parameters: $\lambda_1 = 0.2$, $\lambda_2 = 1$, $a_{cr} = 0.8$.

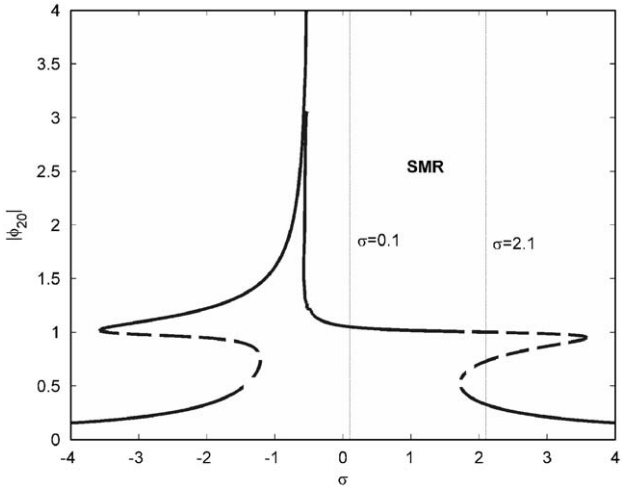

Fig. 12. Frequency-response diagram ($A = 1.2$, $\lambda_1 = \lambda_2 = 0.2$).

forcing amplitude, $A = 1.2$. Therefore, for the sake of comparison, we plot the frequency-response diagram for a quadratic damping case (Fig. 12).

As seen from the diagram at Fig. 12, the branch of undesired periodic response merges with the lower branch. As demonstrated in Ref. [27], the coalescence of the branches occurs at about $A \approx 1$. In this case, it is impossible to find an appropriate set of tuning parameters $(\lambda_1, \lambda_2, a_{cr})$ to obey the second principle without changing other system parameters of tuning (e.g., stiffness of strongly nonlinear spring) since the stable periodic attractors appear in the region above a_{cr}. Therefore, despite the fact that an increase in λ_2 value brings about the decrease of the undesired branch, it does not eliminate it entirely. Existence of the stable attractors on the upper region (above a_{cr}) adversely affects the SMR response due to the increased value of damping as compared to the simple quadratic case (Fig. 12). This can be viewed by comparing the regions of the SMR responses between the piecewise-quadratic damping case (Fig. 11d) and the quadratic damping case (Fig. 12). The SMR interval for the quadratic case in Fig. 12 is larger than the one related to the piecewise-quadratic one (Fig. 11d). However, the advantage of piecewise-quadratic damping for the considered case lies in minimizing the frequency band for which the undesired responses may occur. Therefore, the preference for piecewise-quadratic damping on the quadratic one is apparent for a certain range of forcing amplitudes, namely ($A \leqslant 1.05$). A tradeoff exists between the quadratic and piecewise-quadratic cases for relatively high values of the forcing amplitudes, as illustrated in the last example for $A > 1.05$.

There exists an additional option for tuning of the NES comprising the piecewise-quadratic damping—tuning the nonlinear stiffness k. An example for this case is presented in the following section of numerical verifications and simulations. It is always possible (for an arbitrary value of forcing amplitude A) to set up the piecewise-nonlinear damping parameters $(\lambda_1, \lambda_2, a_{cr})$ and the stiffness k to eliminate the undesired branch of the periodic regimes. This can be viewed by realizing that, in the quadratic damping case, it is possible to scale the parameters of damping and nonlinear stiffness for any value of A to obtain the frequency-response curve suitable for ideal tuning (according to all the listed principles). Specifically, the frequency-response curve will contain the branches of both periodic regimes with no coalescence. Therefore, the value of a_{cr} may be picked between the branches of periodic regimes, thus providing a guarantee for fulfillment of all the tuning principles by appropriate choice of λ_1, λ_2 ($\lambda_2 > \lambda_1$). In the current paper, the tuning of piecewise-quadratic damping characteristics is performed under the fixed value of nonlinear stiffness ($k = 4\varepsilon/3$).

5. Numerical verifications and simulations

The goal of this section is to numerically verify the analytical models developed above as well as to check the performance of the piecewise-quadratic damper. For this sake, we study the responses of the systems under investigation in the space of initial conditions with the help of the Monte Carlo method.

In the first three simulations, we generated a random dataset of one hundred random vectors. A vector contains a set of four random numbers z_j, $j = 1 \ldots 4$ (randomly chosen in a range $[-2, 2]$) assigned as initial conditions to the system of (1.1) ($y_1(0) = z_1$; $\dot{y}_1(0) = z_2$; $y_2(0) = z_3$; $\dot{y}_2(0) = z_4$). Thus, each vector constitutes the initial condition for Eq. (1) which is integrated numerically. Therefore, the original system (Eq. (1)) is subjected to one hundred initial conditions for some fixed value of the frequency detuning σ and other parameters. Frequency detuning σ is varied with a constant step of 0.1 and, for each step of σ, the initial system is integrated for the aforementioned random choice of initial conditions. This simulation was performed both for simple linear damping and for the tuned piecewise-quadratic damping. All simulations for these two cases are illustrated in Figs. 13 and 14, respectively, and numerically derived periodic regimes are marked with circles, while the SMR regime is marked with a diamond. The shade of each marker in Figs. 13

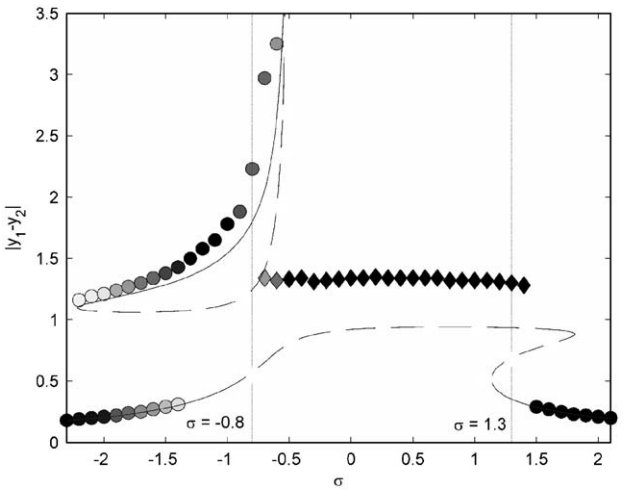

Fig. 13. Numerical simulation for a linear damping case ($A = 0.8$, $\lambda_1 = \lambda_2 = 0.2$, $\varepsilon = 0.01$). SMR regime is denoted with diamonds, periodic regimes are denoted with circles. Thin solid lines refer to analytical solutions of the periodic regimes. The shade of each marker is proportional to the relative number of initial conditions, for which the system is attracted to the particular response regime. Interval of SMR existence is delimited by vertical dashed lines. The WMR was not observed in the simulations.

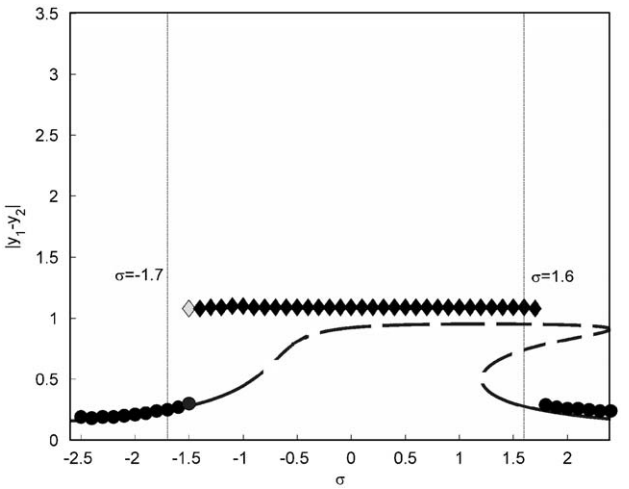

Fig. 14. Numerical simulation for a piecewise-quadratic damping case ($A = 0.8$, $\lambda_1 = 0.2$, $\lambda_2 = 6$, $a_{cr} = 1$, $\varepsilon = 0.01$). SMR regime is denoted with diamonds, periodic regimes are denoted with circles. Thin solid lines refer to analytical solutions of the periodic regimes The shade of each marker is proportional to the relative number of initial conditions, for which the system is attracted to the particular response regime. Interval of SMR existence is delimited by vertical dashed lines. The WMR was not observed in the simulations.

and 14 is proportional to the relative number of initial conditions, for which the system is attracted to the particular response regime. The analytically predicted interval of SMR existence as well as the analytical frequency-response curve of the periodic regimes is also shown in the plots of Figs. 13 and 14. The interval of SMR existence (obtained with the help of the one-dimensional mapping) is delimited by dashed vertical lines on the diagrams. It is also important to emphasize that a weakly modulated response (due to a Hopf bifurcation) was not observed. The deflection in a case of SMR response (marked on the frequency-response diagrams of Figs. 13 and 14 with diamonds) is taken as a maximal relative displacement $y_1 - y_2$.

The results illustrated in the diagrams (Figs. 13 and 14) demonstrate fairly good correspondence between the analytically predicted interval of the SMR response and numerical simulation, and the analytical frequency-response curve of the periodic regimes solutions also agrees with the numeric results.

Comparing the diagram of the linear damping case (Fig. 13) with a piecewise-quadratic one (Fig. 14), one can notice the absence of the branch of undesired periodic response for the piecewise-quadratic damping cases. Thus, only the SMR and the lower branch of the periodic response exist. Because it comes from the diagram of the linear damping case (Fig. 13), there is a certain interval of the frequency band ($\sigma \in [-1.5, -0.7]$) for which the undesired periodic response becomes robust and almost all trajectories of the random initial data are attracted to it. This can be viewed by inspecting the brightness of the markers related to the undesired response branch. Therefore, as long as the branch of the robust undesired periodic response exists, the NES spoils the response instead of improving it. It is apparent from Figs. 13 and 14 that, for a given value of forcing amplitude, piecewise-quadratic damping characteristics substantially improve the performance of the NES by preventing undesired responses.

Up until now, the term ''undesired periodic response'' was somewhat vague, since the branch of the response was presented as the amplitude of the relative displacement between the main mass and the NES ($y_1 - y_2$) vs. frequency. However, when speaking about the vibration suppression, one should be interested in the amplitude of the displacement of the main mass rather then the relative displacement amplitude. In order to demonstrate that the discussed branch of the undesired response is undesired indeed (in a sense of vibration suppression), the frequency-response diagrams were constructed as the amplitude of the main mass (y_1) deflection vs. frequency. Figs. 15 and 16 refer to the linear and piecewise-quadratic damping characteristics, respectively.

Observing the diagram referred to in the linear damping case (Fig. 15), it is clear that the branch of the undesired response corresponds to relatively high amplitudes of the main oscillator. These regimes definitely should be avoided. Unlike the linear damping case, we can see the existence of the beneficial regimes only (SMR and lower branch periodic response) for the case of piecewise-quadratic damping characteristics (Fig. 16).

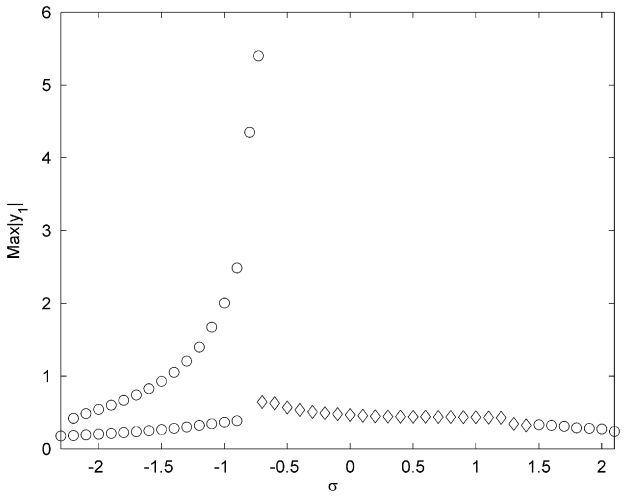

Fig. 15. Numerical simulation for a linear damping case ($A = 0.8$, $\lambda_1 = \lambda_2 = 0.2$, $\varepsilon = 0.01$). SMR regime is denoted with diamonds, periodic regimes are denoted with circles.

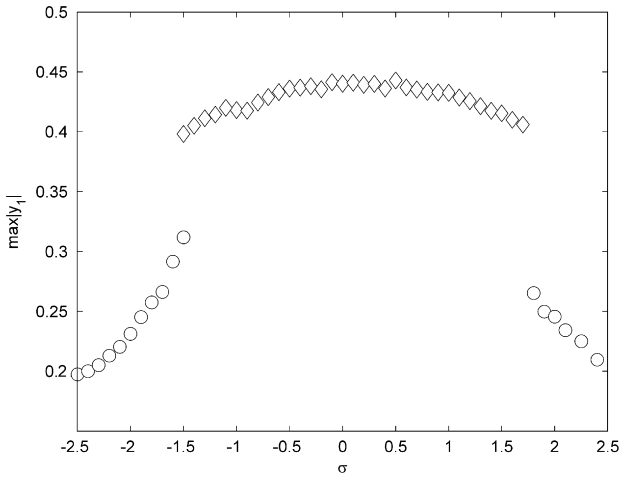

Fig. 16. Numerical simulation for a piecewise-quadratic damping case ($A = 0.8,\ \lambda_1 = 0.2,\ \lambda_2 = 10,\ \varepsilon = 0.01$). SMR regime is denoted with diamonds, periodic regimes are denoted with circles.

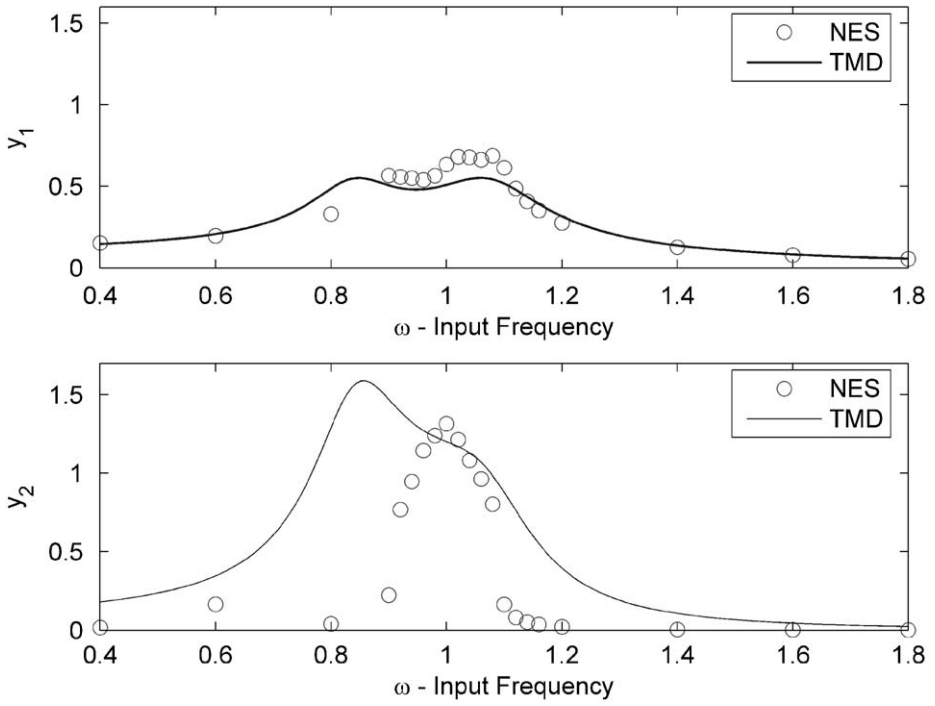

Fig. 17. Frequency-response diagrams for NES and TMD. Response of system with the NES is denoted by circles; the same for the TMD is denoted by a thin line ($A = 0.8,\ \lambda_1 = 0.2,\ \lambda_2 = 10,\ k_a = 4/3,\ a = 1.55,\ \varepsilon = 0.1$).

Comparison of the NES containing piecewise-quadratic damping with a tuned mass damper (TMD, tuned according to Ref. [2]) is illustrated in Figs. 17 and 18 for two distinct values of forcing amplitudes $A = 0.8$; $A = 1.6$, correspondingly.

In order to compare the response regimes of TMD with those of the NES (which may appear with varying amplitude of modulation, e.g., the SMR), the amplitudes were averaged. The results illustrated in Fig. 18 correspond to a relatively high forcing amplitude ($A = 1.6 > 1$). Therefore, as mentioned in the previous

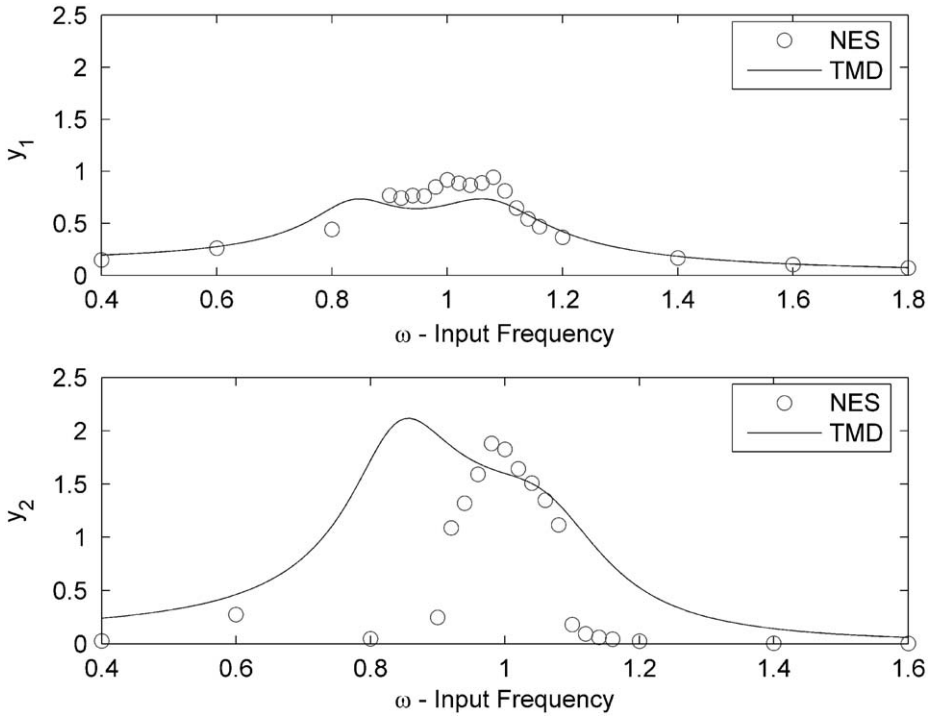

Fig. 18. Frequency-response diagrams for NES and TMD. Response of system with the NES is denoted by circles; the same for the TMD is denoted by a thin line ($A = 1.6$, $\lambda_1 = 0.2$, $\lambda_2 = 10$, $k_a = 0.25$, $a = 2.3$, $\varepsilon = 0.1$).

section, in this case, an optimization of the NES is performed on both nonlinear damping and nonlinear stiffness of the spring (connecting the NES with a primary mass).

As one can see by observing the frequency-response diagrams of Figs. 17 and 18, vibration suppression for the case of the main mass deflection (y_1) is almost the same for both absorbers. However, examining the deflection of absorber (y_2) for both cases (TMD, NES), it is obvious from the diagrams (Figs. 17 and 18) that the NES exhibits essentially lower average displacements. This advantage of the NES arises due to the use of piecewise-quadratic damping.

6. Conclusions

A linear oscillator subject to harmonic excitation (with small amplitude of order ε) and attached to the NES with nonlinear damping has been considered. General analytical treatment was carried out for the system with nonlinear damping of a general type, thus providing the analytical tools used to estimate system response regimes for any particular type of nonlinear damping characteristics. Particular damping characteristics treated in the paper are of the piecewise-quadratic type. It was demonstrated that a properly tuned NES with piecewise-quadratic damping characteristics is able to completely annihilate dangerous periodic regimes arising due to the nonlinearity of the system. Thus, only regimes with efficient vibration absorption (SMR, simple periodic regimes of low amplitudes) remain. Performance of the NES with piecewise-quadratic damping characteristics was compared to the TMD (tuned mass damper). The amount of energy transferred from the main mass (linear oscillator) is almost the same for both absorbers, although the deflection of the NES is much lower than that of the TMD.

It is important to emphasize that the main expected advantage of the NES were observed when it was applied to linear multi-dof systems (with remote frequencies), as demonstrated in Ref. [28]. It was shown that the SMR may be excited in the vicinity of each natural frequency (under excitation), thus providing a substantial reduction of energy for the main mass as compared to the TMD case (which may be tuned to a

single frequency only). However, the major drawback of NES application was the existence of dangerous periodic regimes. The authors believe that the idea presented in this paper of piecewise-quadratic damping will allow the elimination of undesired regimes in the Mdof systems, thus making NES preferable for certain ranges of the forcing amplitudes.

Acknowledgment

The authors are grateful to the Israel Science Foundation (Grant 486/05) for financial support.

Appendix A

In order to show that $a_1(\varphi_2,\varphi_2^*)=\varphi_2 F(|\varphi_2|^2)$, let us consider the definition of $a_1(\varphi_2,\varphi_2^*)$ given in Eq. (5):

$$a_1=\int_0^{2\pi} f(w,\dot{w})\mathrm{e}^{-\mathrm{i}t}\,\mathrm{d}t \tag{A.1}$$

Expressing w, $\dot{w}$ in terms of φ_2,φ_2^* and introducing it into Eq. (A.1), we obtain

$$a_1=\int_0^{2\pi} f\left(-\frac{\mathrm{i}}{2}(\varphi_2\mathrm{e}^{\mathrm{i}t}-\varphi_2^*\mathrm{e}^{-\mathrm{i}t}),\frac{1}{2}(\varphi_2\mathrm{e}^{\mathrm{i}t}+\varphi_2^*\mathrm{e}^{-\mathrm{i}t})\right)\mathrm{e}^{-\mathrm{i}t}\,\mathrm{d}t \tag{A.2}$$

Making the following change of variable:

$$z=\varphi_2\,\mathrm{e}^{\mathrm{i}t} \tag{A.3}$$

Substitution of Eq. (A.3) into Eq. (A.2) provides

$$a_1=-\mathrm{i}\varphi_2\oint_{|Z|=|\varphi_2|} f\left(\frac{-\mathrm{i}}{2}\left(z-\frac{|\varphi_2|^2}{z}\right),\frac{1}{2}\left(z+\frac{|\varphi_2|^2}{z}\right)\right)\frac{\mathrm{d}z}{z^2}=\varphi_2 F(|\varphi_2|^2) \tag{A.4}$$

Appendix B

Algorithm for calculation of an N_x,θ_x pair for the first case ($N_1<a_{cr}<N_2$):

Stage 1: Calculate the N_x value:

N_x value (for the jump from the lower stable branch to the upper one) may be calculated from the polynomials (30, 31) by obeying the invariance of $\varphi_1(\tau)$ related to the fast jump. Thus, exploiting the invariance of the $\varphi_1(\tau)$, one obtains

$$Z_1((1-Z_1)^2+4F^{(1)}(Z_1)^2)=Z_x((1-Z_x)^2+4F^{(2)}(Z_x)^2)=|\varphi_1|^2$$

$$Z_1=N_1^2;\quad Z_x=N_x^2 \tag{B.1}$$

Therefore, the N_x value depends only on N_1. Due to the complexity of Eq. (B.1), the N_x value is calculated numerically (e.g., Newton–Raphson method).

Stage 2: Calculate the θ_x value:

Similarly, using the property of the invariance of $\varphi_1(\tau)$, it is possible to express the θ_x value via N_1, N_x, and θ_0:

$$\theta_x=\tan^{-1}\left(\frac{8\lambda_1 N_1(1-N_x^2)+6\pi F^{(2)}(N_1^2-1)}{3\pi(N_1^2-1)(1-N_x^2)-16\lambda_1 N_1 F^{(2)}}\right)+\theta_0 \tag{B.2}$$

Since N_x is a function of N_1 only, then for each start point on the fold, the angle θ_0 is shifted by a constant value of $\tan^{-1}(8\lambda_1 N_1(1-N_x^2)+6\pi F^{(2)}(N_1^2-1)/3\pi(N_1^2-1)(1-N_x^2)-16\lambda_1 N_1 F^{(1)})$ and the N_1 is mapped to N_x.

Algorithm for calculation of an N_x, θ_x pair for the second case ($N_2 < a_{cr}$):

Stage 1: Calculate the N_x value:

Calculation of the N_x value for the second case ($a_{cr} > N_2$) is not as straightforward as it appeared for the first case. Before we proceed with a final N_x calculation, we should first check the location of the a_{cr} value relative to the unknown N_x value. If the N_x value is situated below the a_{cr} value, then the upper stable branch of the SIM (branch of the trajectory arrival) is not affected by the change in the functional form of F (from $F^{(1)}$ to $F^{(2)}$). On the other hand, if the N_x value is situated above the a_{cr}, then the upper stable branch of the SIM is affected by the change in the functional form of F, and therefore it should be taken into account in the calculation. In that case, an additional stage is added to the algorithm:

Additional stage: Establish the correct location of N_x relative to a_{cr}

First, we verify the location of a_{cr} relative to the N_x calculated for the homogenous functional form (as if there was no change in the functional form of F) of $F = F^{(1)}$ for both the upper and lower branches of SIM. As usual, the N_x value may be calculated by obeying the invariance of $\varphi_1(\tau)$ for the fast jump. Thus, exploiting the invariance of $\varphi_1(\tau)$, one obtains

$$Z_1((1-Z_1)^2 + 4F^{(1)}(Z_1)^2) = Z_x((1-Z_x)^2 + 4F^{(1)}(Z_x)^2) = |\varphi_1|^2$$

$$Z_1 = N_1^2; \quad Z_x = N_x^2 \tag{B.3}$$

Note that, on both sides of Eq. (3.19), we use the same homogenous form of $F = F^{(1)}$. Calculating the intermediate value of N_x, we compare it with the value of a_{cr}. If the value of N_x is lower than a_{cr} ($N_x < a_{cr}$), then algorithm stops and the calculated N_x is the value we are looking for. Otherwise, the value of N_x should be recalculated using Eq. (B.1).

Stage 2: Calculate the θ_x value:

First sub-case ($N_x < a_{cr}$):

Similarly, using the property of the invariance of $\varphi_1(\tau)$, it is possible to express the θ_x value via N_1, N_x, and θ_0:

$$\theta_x = \tan^{-1}\left(\frac{8\lambda_1 N_1(1-N_x^2) + 6\pi F^{(1)}(N_1^2-1)}{3\pi(N_1^2-1)(1-N_x^2) - 16\lambda_1 N_1 F^{(1)}}\right) + \theta_0 \tag{B.4}$$

Since N_x is a function of N_1 only, then for each start point on the fold the angle, θ_0 is shifted by a constant value of $\tan^{-1}(8\lambda_1 N_1(1-N_x^2) + 6\pi F^{(1)}(N_1^2-1)/3\pi(N_1^2-1)(1-N_x^2) - 16\lambda_1 N_1 F^{(1)})$ and the N_1 is mapped to N_x.

Second sub-case ($N_x > a_{cr}$):

In this case, the θ_x value is determined by Eq. (B.2).

The described algorithm contains only the calculations of the jump from lower stable branch of SIM to the upper one. The jump from the upper branch to the lower one is calculated in a similar way. The procedure of numerical integration should be performed twice, for both stable branches of the SIM. Two invariants should be computed for two "fast" jumps in order to determine their final points. It should be stressed that only one computation cycle of the mapping for each point of the initial interval is required. This idea of mapping is close to that used in paper [30] for the analysis of chaotic attractors of relaxation oscillations in the state space of lower dimensionality.

References

[1] H. Frahm, Device for damping vibrations of bodies, U.S. Patent No. 989,958, 1911.
[2] J.P. Den Hartog, *Mechanical Vibrations*, fourth ed., McGraw-Hill Book Company, New York, 1956.
[3] J. Ormondroyd, J.P. Den Hartog, The theory of the dynamic vibration absorber, *Transactions of the American Society of Mechanical Engineers* 50 (1928) A9–A22.
[4] M.N.S. Hadi, Y. Arfiadi, Optimum design of absorber for Mdof structures, *Journal of Structural Engineering* 124 (1998) 1272–1280.
[5] M.P. Singh, L.M. Moreschi, Optimal placement of dampers for passive response control, *Earthquake Engineering & Structural Dynamics* 31 (2002) 955–976.

[6] M.B. Ozer, T.J. Royston, Extending Den Hartog's vibration absorber technique to multi-degree-of-freedom systems, *Journal of Vibration and Acoustics* 127 (4) (2004) 341–350.
[7] R.E. Roberson, Synthesis of a nonlinear dynamic vibration absorber, *Journal of the Franklin Institute* 254 (1952) 205–220.
[8] J. Shaw, S.W. Shaw, A.G. Haddow, On the response of the nonlinear vibration absorber, *International Journal of Non-Linear Mechanics* 24 (1989) 281–293.
[9] H.J. Rice, J.R. McCraith, Practical non-linear vibration absorber design, *Journal of Sound and Vibration* 116 (3) (1987) 545–559.
[10] I.N. Jordanov, I.B. Cheshankov, Optimal design of linear and nonlinear dynamic vibration absorbers, *Journal of Sound and Vibration* 123 (1988) 157–170.
[11] S. Natsiavas, Steady state oscillations and stability of non-linear dynamic vibration absorbers, *Journal of Sound and Vibration* 156 (2) (1992) 227–245.
[12] O.V. Gendelman, Transition of energy to nonlinear localized mode in highly asymmetric system of nonlinear oscillators, *Nonlinear Dynamics* 25 (2001) 237–253.
[13] O.V. Gendelman, A.F. Vakakis, L.I. Manevitch, R. McCloskey, Energy pumping in nonlinear mechanical oscillators I: dynamics of the underlying Hamiltonian system, *Journal of Applied Mechanics* 68 (1) (2001) 34–41.
[14] A.F. Vakakis, O.V. Gendelman, Energy pumping in nonlinear mechanical oscillators II: resonance capture, *Journal of Applied Mechanics* 68 (1) (2001) 42–48.
[15] A.F. Vakakis, Inducing passive nonlinear energy sinks in linear vibrating systems, *Journal of Vibration and Acoustics* 123 (3) (2001) 324–332.
[16] A.F. Vakakis, L.I. Manevitch, O. Gendelman, L. Bergman, Dynamics of linear discrete systems connected to local essentially nonlinear attachments, *Journal of Sound and Vibration* 264 (2003) 559–577.
[17] E. Gourdon, C.H. Lamarque, S. Pernot, Contribution to efficiency of irreversible passive energy pumping with a strong nonlinear attachment, *Nonlinear Dynamics* 50 (2007) 793–808.
[18] E. Gourdon, N.A. Alexander, C.A. Taylor, C.H. Lamarque, S. Pernot, Nonlinear energy pumping under transient forcing with strongly nonlinear coupling: Theoretical and experimental results, *Journal of Sound and Vibration* 300 (2007) 522–551.
[19] Y.S. Lee, A.F. Vakakis, L.A. Bergman, D.M. McFarland, Suppression of limit cycle oscillations in the van der Pol oscillator by means of passive non-linear energy sinks, *Journal of Structural Control and Health Monitoring* 13 (2006) 41–75.
[20] Y.S. Lee, A.F. Vakakis, L.A. Bergman, D.M. McFarland, G. Kerschen, Suppressing aeroelastic instability using broadband passive targeted energy transfers, part 1: theory, *AIAA Journal* 45 (3) (2007).
[21] Y.S. Lee, G. Kerschen, D.M. McFarland, W. Joel Hill, C. Nichkawde, T.W. Strganac, L.A. Bergman, A.F. Vakakis, Suppressing aeroelastic instability using broadband passive targeted energy transfers, part 2: experiments, *AIAA Journal* 45 (3) (2007).
[22] O.V. Gendelman, E. Gourdon, C.H. Lamarque, Quasiperiodic energy pumping in coupled oscillators under periodic forcing, *Journal of Sound and Vibration* 294 (2006) 651–662.
[23] O.V. Gendelman, Y. Starosvetsky, Quasiperiodic response regimes of linear oscillator coupled to nonlinear energy sink under periodic forcing, *Journal of Applied Mechanics* 74 (2007) 325–331.
[24] O.V. Gendeman, Y. Starosvetsky, M. Feldman, Attractors of harmonically forced linear oscillator with attached nonlinear energy sink I: description of response regimes, *Nonlinear Dynamics* 51 (2008) 31–46.
[25] Y. Starosvetsky, O.V. Gendelman, Attractors of harmonically forced linear oscillator with attached nonlinear energy sink II: optimization of a nonlinear vibration absorber, *Nonlinear Dynamics* 51 (2008) 47–57.
[26] Y. Starosvetsky, O.V. Gendelman, Strongly modulated response in forced 2dof oscillatory system with essential mass and potential asymmetry, *Physica D* 237 (2008) 1719–1733.
[27] Y. Starosvetsky, O.V. Gendelman, Response regimes of linear oscillator coupled to nonlinear energy sink with harmonic forcing and frequency detuning, *Journal of Sound and Vibration* 315 (2008) 746–765.
[28] Y. Starosvetsky, O.V. Gendelman, Dynamics of essentially nonlinear vibration absorber coupled to harmonically excited 2 dof system, *Journal of Sound and Vibration* 312 (2008) 234–256.
[29] V.I. Arnold, V.S. Afrajmovich, Yu.S. Il'yashenko, L.P. Shil'nikov, *Dynamical Systems V. Encyclopedia of Mathematical Sciences*, Springer, Berlin, 1994.
[30] J. Guckenheimer, M. Wechselberger, L.-S. Young, Chaotic attractors of relaxation oscillators, *Nonlinearity* 19 (2006) 701–720.
[31] J. Guckenheimer, K. Hoffman, W. Weckesser, Bifurcations of relaxation oscillations near folded saddles, *International Journal of Bifurcations and Chaos* 15 (11) (2005) 3411–3421.
[32] P. Szmolyan, M. Wechselberger, Relaxation oscillations in R^3, *Journal of Differential Equations* 200 (2004) 69–104.
[33] A. Rittweger, J. Albus, E. Hornung, H. Ory, P. Mourey, Passive damping devices for aerospace structures, *Acta Astronautica* 50 (10) (2002) 597–608.
[34] A.A. Golafshani, H.R. Mirdamadi, Adaptive control of structures by LMS algorithm: a comparative study, *Structures and Buildings* 152 (2001) 175–191.